

# DeepNC: Deep Generative Network Completion

Cong Tran, *Student Member, IEEE*, Won-Yong Shin, *Senior Member, IEEE*, Andreas Spitz,  
and Michael Gertz

**Abstract**—Most network data are collected from only partially observable networks with both missing nodes and edges, for example due to limited resources and privacy settings specified by users on social media. Thus, it stands to the reason that inferring the missing parts of the networks by performing *network completion* should precede downstream mining or learning tasks on the networks. However, despite this need, the recovery of missing nodes and edges in such incomplete networks is an insufficiently explored problem. In this paper, we present DeepNC, a novel method for inferring the missing parts of a network that is based on a *deep generative graph* model. Specifically, our model first learns a likelihood over edges via a *recurrent neural network* (RNN)-based generative graph, and then identifies the graph that maximizes the learned likelihood conditioned on the observable graph topology. Moreover, we propose a computationally efficient DeepNC algorithm that consecutively finds a single node to maximize the probability in each node generation step, whose runtime complexity is *almost linear* in the number of nodes in the network. We empirically show the superiority of DeepNC over state-of-the-art network completion approaches on a variety of synthetic and real-world networks.

**Index Terms**—Deep generative graph model; inference; network completion; partially observable network; recurrent neural network (RNN)



## 1 INTRODUCTION

### 1.1 Backgrounds and Motivation

Real-world networks extracted from various biological, social, technological, and information systems tend to be only partially observable and thus missing both nodes and edges [1]. For example, users and organizations may have limited access to data due to insufficient resources or a lack of authority. In social networks, a source of incompleteness stems from privacy settings specified by users who partially or completely hide their identities and/or friendships [2]. As an example, consider a demographic analysis of Facebook users in New York City in June 2011 that showed 52.6% of the users to be hiding the lists of Facebook friends [3]. Using such incomplete network data may severely degrade the performance of downstream analyses such as community detection, link prediction, and node classification due to significantly altered estimates of structural properties (see, e.g., [1], [4], [5], [6] and references therein).

This motivates us to conduct *network completion* to infer the missing part (i.e., a set of both missing nodes and associated edges), prior to performing downstream applications. While intuitively similar, note that network completion fundamentally differs from the well-studied *link prediction*, since it *jointly* infers missing nodes *and* edges. Although there have been attempts that recover both missing nodes and edges, they suffer from several limitations. A state-of-the-art network completion method that aims at inferring the missing part of a network based on the Kronecker graph model, dubbed KronEM [5], suffers from three major problems: 1) setting the size of a Kronecker generative parameter is not trivial; 2) the Kronecker graph model is inherently designed under the assumption of a pure power-law degree distribution that not all real-world networks necessarily follow; and 3) its inference accuracy is not satisfactory yet.

As a way of further enhancing the performance of network completion, our study is intuitively motivated by the existence of *structurally similar* graphs, whose topologies are almost entirely observable.<sup>1</sup> Such similar graphs can be retrieved from the same domain as that of the target graph (see [7], [8], [9] for more information). Suppose that many citizens residing in city A strongly protect the privacy of their social relationships, while citizens of city B tend to provide their friendship relations on social media. Intuitively, as long as the graph structures between two cities are similar to each other, latent information within the (almost) complete

- C. Tran is with the Department of Computer Science and Engineering, Dankook University, Yongin 16890, Republic of Korea and the Department of Computational Science and Engineering, Yonsei University, Seoul 03722, Republic of Korea.  
E-mail: congtran@ieee.org.
- W.-Y. Shin is with the Department of Computational Science and Engineering, Yonsei University, Seoul 03722, Republic of Korea.  
E-mail: wy.shin@yonsei.ac.kr.
- A. Spitz is with the School of Computer and Communication Sciences, cole Polytechnique Fdrale de Lausanne, Lausanne 1015, Switzerland.  
E-mail: andreas.spitz@epfl.ch.
- M. Gertz is with the Institute of Computer Science, Heidelberg University, Heidelberg 69120, Germany.  
E-mail: gertz@informatik.uni-heidelberg.de.

1. Note that in this paper, we use the terms “network” and “graph” interchangeably.

data collected from city B can be uncovered and leveraged to infer the missing part of the collected data from city A. On the other hand, the use of deep learning on graphs has been actively studied by exploiting this structural similarity of graphs (see, e.g., [10], [11] and references therein), which enables us to model complex structures over graphs with a high accuracy. For example, the framework of recurrent neural networks (RNN) and generative adversarial networks (GAN) were recently introduced to construct deep generative models of graphs [10], [11]. Thus, a natural question is how such *structural similarity* can be incorporated into the problem of network completion by taking advantage of effective deep learning-based approaches.

## 1.2 Main Contributions

In this paper, we introduce DeepNC, a novel method for completing the missing part of an observed incomplete network based on a *deep generative graph* model. Specifically, we first learn a likelihood over edges (i.e., a latent representation) via an *RNN-based generative graph* model, termed GraphRNN [10], by using a set of structurally similar graphs as training data, and then infer the missing part of the network. Unlike GraphRNN which is only applicable to fully observable graphs, our method is capable of accommodating both observable and missing parts by imputing a number of missing nodes and edges with *sampled* values from a multivariate Bernoulli distribution. To this end, we formulate a new optimization problem with the aim of finding the graph that maximizes the learned likelihood conditioned on the observable graph topology. To efficiently solve the problem, we propose DeepNC-LC, a low-complexity DeepNC algorithm whose runtime complexity is *almost linear* in the number of nodes. The core insight of underlying DeepNC-LC is to *consecutively* find a single node maximizing the probability in each node generation step in a greedy fashion. Furthermore, we apply judicious approximation and computational reduction techniques to DeepNC-LC by exploiting the *sparseness* of real-world networks. Based on the two performance metrics mean absolute error (MAE) [12] and graph edit distance (GED) [13], we empirically evaluate the performance of DeepNC for various environments. Experimental results show that DeepNC consistently outperforms state-of-the-art network completion approaches by up to 30.55% and 85.15% in terms of MAE and GED, respectively. The results also demonstrate the robustness of our method not only on various real-world networks that do not necessarily follow a power-law degree distribution, but also in two difficult situations where either a large portion of nodes is missing or training graphs are only partially observed. Additionally, we analyze and empirically validate the computational

TABLE 1: Summary of notations

| Notation           | Description  |
|--------------------|--|
| $G_T$              | true graph   |
| $G_O$              | partially observable graph                             |
| $V_O$              | set of nodes in $G_O$                                  |
| $E_O$              | set of edges in $G_O$                                  |
| $V_M$              | set of missing nodes                                   |
| $E_M$              | set of missing edges                                   |
| $G_I$              | training graph   |
| $p_{\text{model}}$ | probability distribution over edges of a graph         |
| $\Theta$           | parameter of $p_{\text{model}}$                        |
| $\hat{G}$          | recovered graph  |
| $\pi$              | node order   |
| $\mathbf{S}^\pi$   | a sequence of nodes and edges under a node order $\pi$ |

complexity of DeepNC. Our main contributions are five-fold and summarized as follows:

- We introduce DeepNC, a deep learning-based network completion method for partially observable networks;
- We formalize the problem of identifying a node order that maximizes the conditional probability of a generated node sequence as an optimization problem;
- We design a computationally efficient DeepNC algorithm to solve the problem by exploiting a sparse structure of networks;
- We validate DeepNC through extensive experiments using real-world datasets across various domains, as well as synthetic datasets;
- We analyze and empirically validate computational complexity of DeepNC.

To the best of our knowledge, this study is the first work that applies deep learning to network completion.

## 1.3 Organization and Notations

The remainder of this paper is organized as follows. In Section 2, we summarize significant studies that are related to our work. In Section 3, we explain the methodology of our work, including the problem definition and an overview of our DeepNC method. Section 4 describes implementation details of our DeepNC-LC approach. Experimental results are discussed in Section 5. Finally, we provide a summary and concluding remarks in Section 6.

Table 1 summarizes the notation that is used in this paper. This notation will be formally defined in the following sections when we introduce our methodology and the technical details.

## 2 RELATED WORK

The method that we propose in this paper is related to two broader areas of research, namely generative graph models and network completion.

**Generative graph models.** The study of generative graph models has a long history, beginning with the first random graph model that robustly assigns probabilities to large classes of graphs, and was introduced by Erdős and Rényi [14]. Another well-known model allows a node to have a high likelihood to be connected to new nodes added to the underlying graph if the node is highly connective [15]. More recently, a generative graph model based on Kronecker graphs, the so-called KronFit, was introduced in [16], which generates synthetic networks that have structural properties of real-world networks. Recent advances in *deep learning*-based approaches have made further progress towards generative models for complex networks [10], [11], [17], [18], [19], [20]. GraphRNN was presented to learn a distribution over edges by decomposing the graph generation process into sequences of node and edge formations via an RNN-based generative graph model [10]; generative adversarial networks (GANs) using the Wasserstein GAN objective in the training process were applied to generate discrete output samples [11]; another deep learning-based generative graph model was introduced by employing a variational autoencoder [17]; a graph convolutional policy network was presented for goal-directed graph generation (e.g., drug molecules) using reinforcement learning [18]; a multi-scale graph generative model, named Misc-GAN, was introduced by modeling the underlying distribution of graph structures at different levels of granularity to aim at generating graphs having similar community structures [19]; and a more general deep generative model was presented to learn distributions over any arbitrary graph via graph neural networks [20].

**Network completion.** Observing a partial sample of a network and inferring the remainder of the network is referred to as *network completion*. As the most influential study, KronEM, an approach based on Kronecker graphs to solving the network completion problem by applying the expectation-maximization (EM) algorithm, was suggested by Kim and Leskovec [5]. For cases in which only a small number of edges are missing, vertex similarity [21] was shown to be useful in recovering the underlying true network. Another method for inferring missing edges in social networks based on shared node neighborhoods was investigated by Buccafurri et al. [22]. MISC was developed to tackle the *missing node identification* problem when the information of connections between missing nodes and observable nodes is assumed to be available [23]. A follow-up study of

MISC [24] attempted to incorporate side information such as the demographic information and the nodes historical behavior into the inference process.

**Discussions.** Despite these contributions, there has been no prior work in the literature that exploits the power of deep generative models in the context of network completion. We find that generative graph models themselves such as GraphRNN can be used as a network completion method with a nontrivial extra task. More specifically, a graph generated by a deep generative graph model needs to undergo a *graph matching* process due to the lack of correspondence between generated nodes and observable nodes. Since graph matching is computationally expensive (e.g., a typical method has the complexity of  $\mathcal{O}(N^6)$ , where  $N$  denotes the number of nodes in a graph [25]), incorporating such an idea into GraphRNN would be highly inefficient. Furthermore, MISC and other follow-up studies do not truly address network completion, since they solve the *node identification* problem under the assumption that the connections between missing nodes and observable nodes are known beforehand, which is not feasible in our partial observation setting.

## 3 METHODOLOGY

As a basis for the proposed DeepNC algorithm in Section 4, we first describe our network model with basic assumptions and formulate our problem. Then, we explain a deep generative graph model and our research methodology adopting the deep generative graph model to solve the problem of network completion.

### 3.1 Problem Definition

#### 3.1.1 Network Model and Basic Assumptions

Let us denote a partially observable network as  $G_O = (V_O, E_O)$ , where  $V_O$  and  $E_O$  are the set of vertices and the set of edges, respectively. The network  $G_O$  with  $|V_O|$  observable nodes can be interpreted as a subgraph taken from an underlying true network  $G_T = (V_O \cup V_M, E_O \cup E_M)$ , where  $V_M$  is the set of unobservable (missing) nodes and  $E_M$  is the set of unobservable (missing) edges including not only the edges connecting two nodes in  $V_M$  but also the edges connecting one node in  $V_O$  and another node in  $V_M$ . As in [5], we assume that there is no missing edge between two nodes in  $V_O$ , which implies that  $G_O$  is a complete subgraph. In the following, we assume both  $G_O$  and  $G_T$  to be *undirected unweighted* networks without self-loop and repeated edges.

Let us denote  $p_{\text{model}}$  as a family of probability distributions over the edges of a graph, which can be parameterized by a set of parameters  $\Theta$ , i.e.,  $(p_{\text{model}}^\Theta; \Theta)$ . In this paper, we

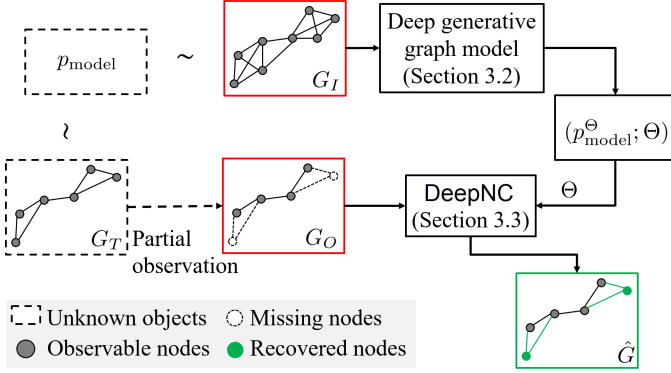


Fig. 1: The schematic overview of our DeepNC method.

suppose that  $G_T$  is a sample drawn from the distribution  $p_{\text{model}}$ . Furthermore, we assume that the number of missing nodes,  $|V_M|$ , is either known or can be approximated by standard methods for estimating the size of hidden or missing populations by fitting a statistical model of the population based on a number of sampled surveys [26]. Some network-relevant notations above are depicted in Fig. 1.

### 3.1.2 Problem Formulation

In what follows, we formally state the network completion problem, the idea behind our approach, and the problem formulation.

**Definition 1. Network completion problem [5].** *Given a partially observable network  $G_O$ , network completion aims to infer the connections of  $|V_M|$  missing nodes to the nodes in  $V_O$  and the connections among missing nodes so that the inferred network, denoted by  $\hat{G}$ , is isomorphic to the true network  $G_T$ .*

As illustrated in Fig. 1, a network  $\hat{G}$  (depicted by a green rectangle) is inferred using the partially observable network  $G_O$  as input of DeepNC (depicted by a red rectangle). We tackle this problem in the sense of minimizing a distance metric  $D(G_T, \hat{G})$  that measures the difference between  $G_T$  and  $\hat{G}$ . Due to the fact that the true network  $G_T$  is not available, our main idea behind this problem is to analyze the connectivity patterns of one (or multiple) fully observed network(s)  $G_I$  whose structure is similar to that of  $G_T$  and then to make use of such information for recovering the network  $G_O$ , where  $G_I$  is a sample drawn from the distribution  $p_{\text{model}}$ .<sup>2</sup> To this end, we first learn  $(p_{\text{model}}^\Theta; \Theta)$  by using  $G_I$  as the *training* data under a deep generative graph model described in Section 3.2. Afterwards, we generate graphs with similar structures via the set of learned parameters  $\Theta$ . Among all generated graphs  $G$ , we find the most likely graph configuration  $\hat{G}$  given the observable part  $G_O$ . In

2. The number of nodes in  $G_I$  should be greater than or equal to that in  $G_T$  so that the information (i.e., the distribution  $p_{\text{model}}^\Theta$ ) encoded by learned parameters  $\Theta$  is sufficient to infer  $G_T$ .

this context, our optimization problem can be formulated as follows:

$$\hat{G} = \arg \max_G P(G|G_O, \Theta). \quad (1)$$

The overall procedure of our approach is visualized in Fig. 1.

## 3.2 Deep Generative Graph Model

Deep generative graph models have the ability to approximate any distribution of graphs with minimal assumptions about their structures. Among recently introduced deep generative graph models, GraphRNN [10] is adopted in our study due to the outstanding performance in generating diverse graphs that match the structural characteristics of a target set as well as the scalability to much larger graphs than those from other deep generative graph models. In this subsection, we elaborate on the method built upon a variant of GraphRNN, which characterizes the probability of a graph and learns  $(p_{\text{model}}^\Theta; \Theta)$  from the set of *structurally similar network(s)*  $G_I$ .

We first describe how to vectorize a graph. Given a graph  $G$  having  $|V_O| + |V_M|$  nodes, we define node order  $\pi$  that maps nodes to rows or columns of a given adjacency matrix of  $G$  as a permutation function over the set of nodes, i.e.,  $\{\pi(v_1), \dots, \pi(v_{|V_O|+|V_M|})\}$  that is a permutation of  $\{v_1, \dots, v_{|V_O|+|V_M|}\}$ , thus yielding  $(|V_O|+|V_M|)!$  possible node permutations. Then, a sequence  $\mathbf{S}$  given a node order  $\pi$  is defined as follows:

$$\mathbf{S}^\pi \triangleq (\mathbf{S}_1^\pi, \dots, \mathbf{S}_{|V_O|+|V_M|}^\pi), \quad (2)$$

where each element  $\mathbf{S}_i^\pi \in \{0, 1\}^{i-1}$  for  $i \in \{2, \dots, |V_O| + |V_M|\}$  is a binary adjacency vector representing the edges between node  $\pi(v_i)$  and the previous nodes  $\pi(v_j)$  for  $j \in \{1, \dots, i-1\}$  that already exist in the graph and  $\mathbf{S}_1^\pi = \emptyset$ . Here,  $\mathbf{S}_i^\pi$  can be expressed as

$$\mathbf{S}_i^\pi = (a_{1,i}^\pi, \dots, a_{i-1,i}^\pi), \quad \forall i \in \{2, \dots, |V_O| + |V_M|\}, \quad (3)$$

where  $a_{u,v}^\pi$  denotes the  $(u, v)$ -th element of the adjacency matrix  $\mathbf{A}^\pi \in \{0, 1\}^{(|V_O|+|V_M|) \times (|V_O|+|V_M|)}$  for  $u, v \in \{1, \dots, |V_O| + |V_M|\}$  (refer to Fig. 2 for an illustration of the sequence). Due to the fact that the graphs are discrete objects, the graph generation process should involve discrete decisions that are not differentiable and therefore problematic for back propagation. Thus, instead of directly learning the distribution  $p(G)$ , we sample a node order  $\pi$  from the set of  $(|V_O| + |V_M|)!$  node orders to generate the sequences  $\mathbf{S}^\pi$  and learn the distribution  $p(\mathbf{S}^\pi)$ .

Next, we explain how to characterize the probability  $p(\mathbf{S}^\pi)$ . Due to the sequential nature of  $\mathbf{S}^\pi$ , the probability  $p(\mathbf{S}^\pi)$  can be decomposed as the product of conditional

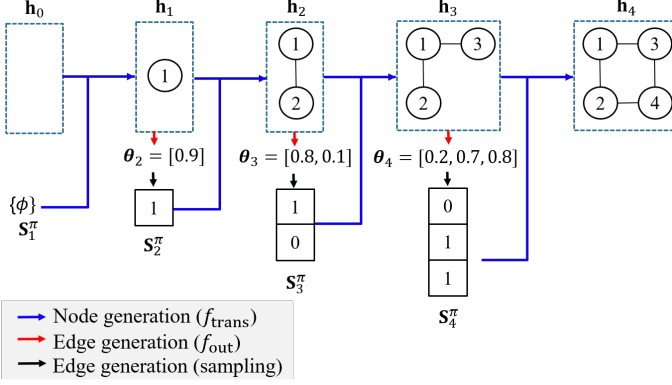


Fig. 2: An example illustrating the inference process of GraphRNN. Here, the blue arrows denote the graph-level RNN that encodes the “graph state” vector  $\mathbf{h}_i$  in its hidden state, and the red and black arrows represent the edge generation process whose input is given by the graph-level RNN.

probability distributions over the elements as in the following:

$$p(\mathbf{S}^\pi) = \prod_{i=2}^{|V_O|+|V_M|} p(\mathbf{S}_i^\pi | \mathbf{S}_1^\pi, \dots, \mathbf{S}_{i-1}^\pi). \quad (4)$$

For ease of presentation, we simplify  $p(\mathbf{S}_i^\pi | \mathbf{S}_1^\pi, \dots, \mathbf{S}_{i-1}^\pi)$  as  $p(\mathbf{S}_i^\pi | \mathbf{S}_{<i}^\pi)$  for the rest of the paper. Assuming that the probability of edges for a node is independent of each other, we can further decompose  $p(\mathbf{S}_i^\pi | \mathbf{S}_{<i}^\pi)$  into the product of conditional probability distributions as follows:

$$p(\mathbf{S}_i^\pi | \mathbf{S}_{<i}^\pi) = \prod_{j=1}^{i-1} p(s_{i,j}^\pi | \mathbf{S}_{<i}^\pi), \quad (5)$$

which results in

$$p(\mathbf{S}^\pi) = \prod_{i=2}^{|V_O|+|V_M|} \prod_{j=1}^{i-1} p(s_{i,j}^\pi | \mathbf{S}_{<i}^\pi), \quad (6)$$

where  $s_{i,j}^\pi$  denotes the  $j$ -th element of the vector  $\mathbf{S}_i^\pi$  for  $i \in \{2, \dots, |V_O| + |V_M|\}$  and  $j \in \{1, \dots, i-1\}$ .

Now, let us turn to describing the use of RNN in generating a sequence  $\mathbf{S}^\pi$  from the training network(s)  $G_I$ . The main idea behind the RNN model is to decompose graph generation into a process generating a sequence of nodes (via the so-called graph-level RNN) and another process generating edges for each newly added node. To this end, GraphRNN aims to learn two functions  $f_{\text{trans}}$  and  $f_{\text{out}}$  that are used in each generation step according to the following procedure (refer to Fig. 2). We denote  $\mathbf{h}_i \in \mathbb{R}^d$  as a graph state vector representing the hidden state of the model in the  $i$ -th step, where  $d \in \mathbb{N}$  is a user-defined parameter that is typically set to a value smaller than  $|V_O| + |V_M|$ . A state-transition function  $f_{\text{trans}}$  is used to compute the graph state vector  $\mathbf{h}_i$  based on both the previous hidden state  $\mathbf{h}_{i-1}$  and

the input  $\mathbf{S}_i^\pi$ , and is given by

$$\mathbf{h}_i = f_{\text{trans}}(\mathbf{h}_{i-1}, \mathbf{S}_i^\pi). \quad (7)$$

Intuitively,  $\mathbf{h}_i$  encodes the topological information of  $i$  generated nodes in a low-dimensional vector representation. The first generation step involves a randomly initialized  $\mathbf{h}_0$  and  $\mathbf{S}_1^\pi = \emptyset$  to produce  $\mathbf{h}_1$ . Then, as the output of the  $i$ -th step of GraphRNN, an output function  $f_{\text{out}}$  is invoked to obtain a vector  $\boldsymbol{\theta}_{i+1} \in (0, 1)^i$  specifying the distribution of the next node’s adjacency vector as follows:

$$\boldsymbol{\theta}_{i+1} = f_{\text{out}}(\mathbf{h}_i). \quad (8)$$

Following a variant of GraphRNN in [10], we model  $p(\mathbf{S}_i^\pi | \mathbf{S}_{<i}^\pi)$  as a multivariate Bernoulli distribution parametrized by  $\boldsymbol{\theta}_i$ . Thus, every entry of  $\boldsymbol{\theta}_i$  in (8) can be interpreted as a probability representing whether there exists an edge between nodes  $i$  and  $j$  for  $j \in \{1, \dots, i-1\}$ . As we can sample edges in  $\mathbf{S}^\pi$  independently according to a multivariate Bernoulli distribution parametrized by  $\boldsymbol{\theta}_i$ , the probability  $p(\mathbf{S}_i^\pi | \mathbf{S}_{<i}^\pi)$  can then be computed as

$$p(\mathbf{S}_i^\pi | \mathbf{S}_{<i}^\pi, \boldsymbol{\theta}_i) = \prod_{s_{i,j}^\pi=1} \boldsymbol{\theta}_i[j] \prod_{s_{i,j}^\pi=0} (1 - \boldsymbol{\theta}_i[j]), \quad (9)$$

where  $\boldsymbol{\theta}_i[j] \in (0, 1)$  is the  $j$ -th element of  $\boldsymbol{\theta}_i$ . When  $\Theta = \{\boldsymbol{\theta}_2, \dots, \boldsymbol{\theta}_{|V_O|+|V_M|}\}$ , the probability of a sequence given  $\Theta$  is computed as follows:

$$p(\mathbf{S}^\pi; \Theta) = \prod_{i=2}^{|V_O|+|V_M|} \left( \prod_{s_{i,j}^\pi=1} \boldsymbol{\theta}_i[j] \prod_{s_{i,j}^\pi=0} (1 - \boldsymbol{\theta}_i[j]) \right). \quad (10)$$

We note that the entries in  $\boldsymbol{\theta}_i$  are obtained via two neural networks  $f_{\text{trans}}$  and  $f_{\text{out}}$ —the function  $f_{\text{trans}}$  can be found via general neural networks such as gated recurrent units (GRUs) [27] or long short-term memory units [28] in RNN and the function  $f_{\text{out}}$  can be an ordinary neural network. The weights of  $f_{\text{trans}}$  and  $f_{\text{out}}$  are optimized using training sequences sampled from  $G_I$  (refer to [10] for more details of the training process). Fig. 2 illustrates the inference process of GraphRNN, where a graph consisting of four nodes is generated as depicted from left to right. In more details, after obtaining  $\boldsymbol{\theta}_2$  via (7) and (8),  $\mathbf{S}_2^\pi = [1]$  is acquired by sampling from the multivariate Bernoulli distribution parameterized by  $\boldsymbol{\theta}_2$ , which means that the next generated node (i.e., node 2) is linked to node 1. Following a similar procedure, we obtain  $\mathbf{S}_3^\pi = [1, 0]$  and  $\mathbf{S}_4^\pi = [0, 1, 1]$  representing the connections of nodes 3 and 4 with previously generated nodes, respectively.

### 3.3 Network Completion

In this subsection, we present our DeepNC method that recovers the missing part of the true network  $G_T$  based on

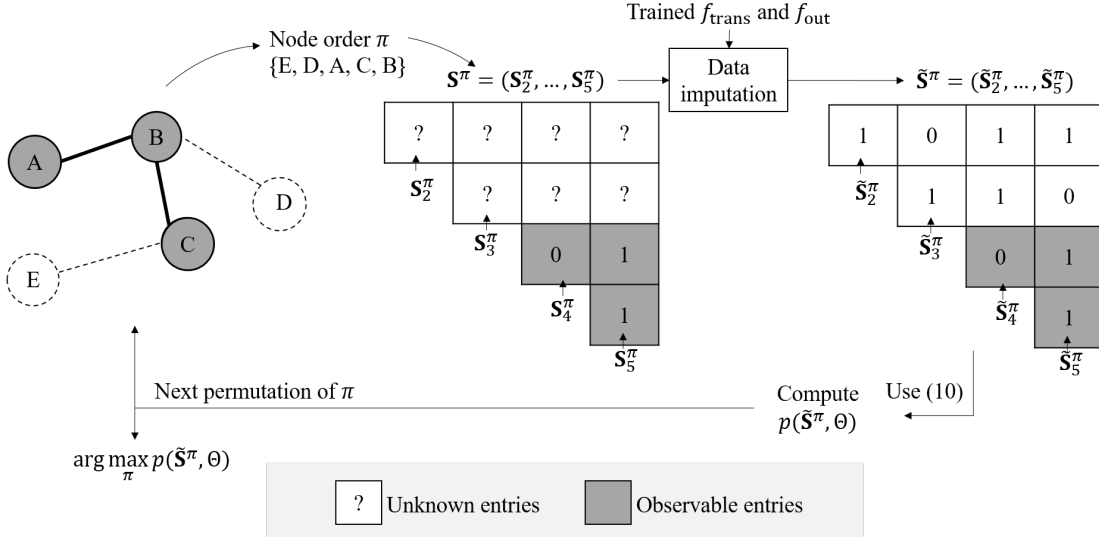


Fig. 3: An example illustrating the schematic overview of our DeepNC method, where three nodes (i.e., A, B, and C) and two edges with solid lines are observable instead of the true graph  $G_T$  consisting of five nodes and all associated edges.

the deep generative graph model. We first introduce the approach that seamlessly accommodates both observable and missing parts of  $G_T$  into the graph generation process of GraphRNN, and then present a new form of problem formulation built upon (1).

More specifically, by modeling graphs as sequences presented in Section 3.2, we reformulate our optimization problem in (1) in the sense of finding a sequence  $\hat{\mathbf{S}}^\pi$  that maximizes  $p(\mathbf{S}^\pi | G_O, \Theta)$  under a node order  $\pi$  as follows:

$$\hat{\mathbf{S}}^\pi = \arg \max_{\mathbf{S}^\pi} p(\mathbf{S}^\pi | G_O, \Theta). \quad (11)$$

Next, we apply an *imputation* strategy of the missing data (i.e., unknown entries) in the sequence  $\mathbf{S}^\pi$  to our DeepNC method. Under a node order  $\pi$ , as a sequence  $\mathbf{S}^\pi$  contains both unknown and observable entries representing edges in the sets  $E_M$  and  $E_O$ , respectively (see Fig. 3), the sequence through the data imputation process, denoted by  $\hat{\mathbf{S}}^\pi$ , contains both the observable entries taken directly from  $\mathbf{S}^\pi$  and the entries imputed via the inference process of GraphRNN using trained  $f_{\text{trans}}$  and  $f_{\text{out}}$ . To be specific, suppose that  $\pi(u) = i$  and  $\pi(v) = j$ , which means that the  $i$ -th and  $j$ -th nodes in a given node order  $\pi$  are  $u$  and  $v$ , respectively. Then, we have

$$\tilde{s}_{ij}^\pi = \begin{cases} \text{Bernoulli}(\theta_i[j]), & \text{if } u \notin V_O \text{ or } v \notin V_O \\ s_{i,j}^\pi, & \text{otherwise,} \end{cases} \quad (12)$$

where  $\tilde{s}_{ij}^\pi$  denotes the  $j$ -th element of the binary vector  $\tilde{\mathbf{S}}_i^\pi$  for  $i \in \{2, \dots, |V_O| + |V_M|\}$  and  $j \in \{1, \dots, i-1\}$ ; and the Bernoulli trial with the probability  $\theta_i[j]$  maps the value of the unknown entry to one if the outcome “success” occurs and to zero otherwise. Then, the optimization problem in

(11) is equivalent to

$$\hat{\mathbf{S}}^\pi = \arg \max_{\mathbf{S}^\pi} p(\tilde{\mathbf{S}}^\pi; \Theta),$$

which can further be simplified to

$$\hat{\pi} = \arg \max_{\pi} p(\tilde{\mathbf{S}}^\pi; \Theta), \quad (13)$$

since  $\tilde{\mathbf{S}}^\pi$  is sampled from the set of all node orders. An example visualizing our DeepNC method is presented in Fig. 3, where we observe a network  $G_O$  consisting of three nodes (i.e., A, B, and C) and two edges, instead of the true network  $G_T$  with 5 nodes (i.e., A, B, C, D, and E). This problem can be solved by computing  $p(\tilde{\mathbf{S}}^\pi; \Theta)$  via exhaustive search over  $(|V_O| + |V_M|)!$  node permutations. Since computing  $p(\tilde{\mathbf{S}}^\pi; \Theta)$  in (10) requires  $\frac{(|V_O| + |V_M|)^2}{2}$  multiplication operations, its computational complexity is bounded by  $\mathcal{O}((|V_O| + |V_M|)^2(|V_O| + |V_M|)!)$ . This motivates us to introduce a low-complexity algorithm for efficiently solving such a problem in the next section.

## 4 LOW-COMPLEXITY DEEPCNC ALGORITHM

We first describe our low-complexity DeepNC algorithm and then show its computational complexity.

### 4.1 Algorithm Description

#### 4.1.1 Algorithm Overview

In this subsection, we propose DeepNC-LC, a low-complexity network completion algorithm that approximates the optimal solution to the objective function in (11) by selecting nodes in the graph generation process in a greedy manner. To this end, instead of exhaustively

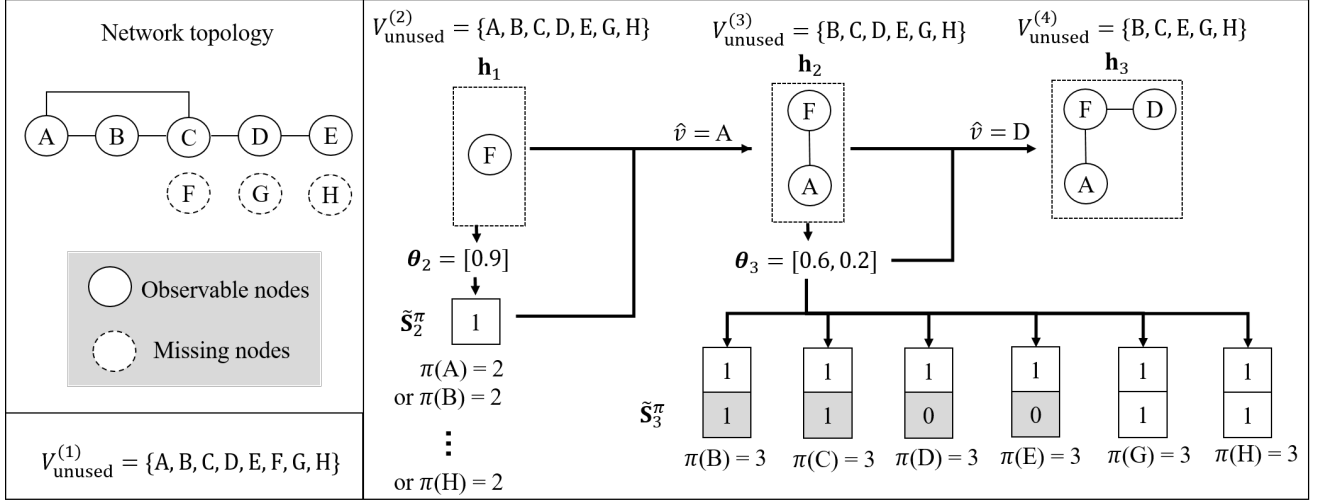


Fig. 4: An example illustrating the mechanism of DeepNC-LC, where the first three steps are shown.

searching for the node order maximizing  $p(\tilde{\mathbf{S}}^\pi, \Theta)$  among  $(|V_O| + |V_M|)!$  possible outcomes, we aim at *consecutively* finding a single node  $\hat{v}$  that maximizes  $p(\tilde{\mathbf{S}}_i^\pi | \tilde{\mathbf{S}}_{<i}^\pi, \theta_i)$  in each inference step  $i$ , subject to  $\pi(\hat{v}) = i$  for  $i \in \{2, \dots, |V_O| + |V_M|\}$ , where  $\pi(\hat{v}) = i$  indicates that the  $i$ -th node in a given node order  $\pi$  is  $\hat{v}$ .<sup>3</sup> More specifically, when we denote  $V_{\text{unused}}^{(i)}$  as the set of nodes that can be potentially generated in the  $i$ -th step of the algorithm, we find the node  $\hat{v}$  such that

$$\hat{v} = \arg \max_{v \in V_{\text{unused}}^{(i)}} p(\tilde{\mathbf{S}}_i^\pi | \tilde{\mathbf{S}}_{<i}^\pi, \theta_i) \quad (14)$$

subject to  $\pi(v) = i$

for each step  $i \in \{2, \dots, |V_O| + |V_M|\}$ , where  $\hat{v}$  is removed from  $V_{\text{unused}}^{(i)}$  after each inference step (that is,  $V_{\text{unused}}^{(i+1)} \leftarrow V_{\text{unused}}^{(i)} \setminus \{\hat{v}\}$ ). Initially, when  $i = 1$ , we set  $V_{\text{unused}}^{(1)}$  to  $V_O \cup V_M$ , and choose a random node in  $V_{\text{unused}}^{(1)}$  to be the first node of the inference process. We then exclude the first node from  $V_{\text{unused}}^{(1)}$  to create  $V_{\text{unused}}^{(2)}$  and repeat the node search in (14)  $|V_O| + |V_M| - 1$  times until the recovered graph is fully generated. For better understanding, we present a motivating example as follows.

**Example 1:** As depicted in Fig. 4, let us describe three steps to select the first three nodes of a given graph according to (14). We start by randomly assigning the first node of the inference process to node F (i.e.,  $\pi(F) = 1$  and  $V_{\text{unused}}^{(2)} \leftarrow V_{\text{unused}}^{(1)} \setminus \{F\}$ ). Since we do not have any information about the connections for the unseen node F,  $s_{2,1}^\pi$  is unknown for all nodes  $v \in V_{\text{unused}}^{(2)}$ . Assuming that  $\theta_2 = [0.9]$  and all Bernoulli trials with the probability  $\theta_2$  for all  $v \in V_{\text{unused}}^{(2)}$  return 1, we impute  $\tilde{s}_{2,1}^\pi$  with 1 according to (12). Then, from (9), it follows that  $p(\tilde{\mathbf{S}}_2^\pi | \tilde{\mathbf{S}}_{<2}^\pi, \theta_2) = 0.9$  for  $\forall v \in V_{\text{unused}}^{(2)}$ , which implies that all the remaining nodes in

$V_{\text{unused}}^{(2)}$  yield the same likelihood in (14). In this example, we randomly choose node A among the seven nodes in  $V_{\text{unused}}^{(2)}$  as the second node and set  $\pi(A) = 2$ , resulting in  $V_{\text{unused}}^{(3)} \leftarrow V_{\text{unused}}^{(2)} \setminus \{A\}$ . Let us turn to the next step in order to select the third node. In this case, since nodes B, C, D, and E belong to the observable nodes,  $\tilde{s}_{3,2}^\pi$  takes the value of either *one* or *zero*, depending on the connections with node A, when either  $\pi(v_1)$  or  $\pi(v_2)$  is set to 3, respectively, where  $v_1 \in \{B, C\}$  and  $v_2 \in \{D, E\}$  (refer to Fig. 4). When we suppose that  $\theta_3 = [0.6, 0.2]$  and all Bernoulli trials with the probability  $\theta_3[j]$  for all  $v \in V_{\text{unused}}^{(3)}$  and  $j \in \{1, 2\}$  return 1, the likelihood  $p(\tilde{\mathbf{S}}_3^\pi | \tilde{\mathbf{S}}_{<3}^\pi, \theta_3)$  in (14) can be computed as follows:

- If either  $\pi(B) = 3$  or  $\pi(C) = 3$ , then we impute  $\tilde{s}_{3,1}^\pi$  with 1 and assign  $\tilde{s}_{3,2}^\pi = s_{3,2}^\pi = 1$  according to (12). Thus, we have  $\tilde{\mathbf{S}}_3^\pi = [1, 1]$  and  $p(\tilde{\mathbf{S}}_3^\pi | \tilde{\mathbf{S}}_{<3}^\pi, \theta_3) = \theta_3[1]\theta_3[2] = 0.6 \times 0.2 = 0.12$  using (9).
- If either  $\pi(D) = 3$  or  $\pi(E) = 3$ , then we have  $\tilde{\mathbf{S}}_3^\pi = [1, 0]$  and  $p(\tilde{\mathbf{S}}_3^\pi | \tilde{\mathbf{S}}_{<3}^\pi, \theta_3) = \theta_3[1](1 - \theta_3[2]) = 0.6 \times (1 - 0.2) = 0.48$  in a similar manner.
- If either  $\pi(G) = 3$  or  $\pi(H) = 3$ , then  $\tilde{\mathbf{S}}_3^\pi = [1, 1]$  and  $p(\tilde{\mathbf{S}}_3^\pi | \tilde{\mathbf{S}}_{<3}^\pi, \theta_3) = \theta_3[1]\theta_3[2] = 0.6 \times 0.2 = 0.12$ .

Based on the above results, setting either  $\pi(D)$  or  $\pi(E)$  to 3 leads to the maximum value of  $p(\tilde{\mathbf{S}}_3^\pi | \tilde{\mathbf{S}}_{<3}^\pi, \theta_3)$ , which is thus the solution to the problem in (14) for  $i = 3$ . As depicted in Fig. 4, node D is randomly chosen in this step.

#### 4.1.2 Efficient Computation

From now on, we turn to examining how to efficiently compute the likelihoods in the inference process through some judicious approximation and computational reduction techniques. From Example 1, it is worth noting that all unobservable entries in  $\tilde{\mathbf{S}}_i^\pi$  have been treated *equally* in

3. The first node can be arbitrarily chosen in the generation process.

computation for the case where all Bernoulli trials return 1. Thus, rather than computing the likelihoods in (14) along with all entries in  $\tilde{\mathbf{S}}_i^\pi$ , we apply an approximation strategy to node selection in the graph generation process.

First, we select the *node type* (i.e., either missing nodes or observable nodes) at random in *proportion to the number of nodes for each type* in the set  $V_{\text{unused}}^{(i)}$  to ensure that there is no bias in the node selection. Then, when the selected node type is “missing”, we choose a missing node at random from missing nodes in  $V_{\text{unused}}^{(i)}$  without any computation since all unobservable nodes are treated equally. In contrast, when the selected node type is “observable”, we choose an observable node based solely on computation for the observable entries in  $\mathbf{S}_i^\pi$  by reformulating the problem in (14) as follows:

$$\begin{aligned} \hat{v} = \arg \max_{v \in V_O \cap V_{\text{unused}}^{(i)}} p(\mathbf{O}_i^\pi | \tilde{\mathbf{S}}_{<i}^\pi, \boldsymbol{\theta}_i) \\ \text{subject to } \pi(v) = i, \end{aligned} \quad (15)$$

where  $\mathbf{O}_i^\pi$  denotes the set of observable entries in  $\mathbf{S}_i^\pi$ ;  $p(\mathbf{O}_i^\pi | \tilde{\mathbf{S}}_{<i}^\pi, \boldsymbol{\theta}_i) = \prod_{s_{i,j}^\pi=1} \boldsymbol{\theta}_i[j] \prod_{s_{i,j}^\pi=0} (1 - \boldsymbol{\theta}_i[j])$  from (9); and  $V_O \cap V_{\text{unused}}^{(i)}$  indicates the set of remaining observable nodes after  $i - 1$  inference steps. Unlike the original approach based on (14), this new problem formulation allows us to select each node *before data imputation* of the missing data.

Now, let us make a useful observation illustrated in Fig. 5 in order to further reduce the computational complexity. Suppose that nodes X, A, B, and E from the original graph with 8 observable nodes and 3 missing nodes have been generated sequentially after four inference steps, as depicted in Fig. 5. Then, one can see that  $\mathbf{O}_5^\pi$  is given by zeros when node D, G, or H is selected in the fifth step (i.e.,  $\pi(D) = 5$ ,  $\pi(G) = 5$ , or  $\pi(H) = 5$ ) since each of the three nodes has no connection to the nodes A, B, and E that have already been generated. Consequently, the likelihood  $p(\mathbf{O}_5^\pi | \tilde{\mathbf{S}}_{<5}^\pi, \boldsymbol{\theta}_5)$  is identical for these three cases. To generalize this finding, we would like to establish the following lemma.

**Lemma 1.** *Let  $L^{(i)}$  denote the set of “nonselected” direct neighbors of observable nodes generated for  $i - 1$  inference steps, expressed as*

$$L^{(i)} = \begin{cases} (L^{(i-1)} \cup \mathcal{N}(\hat{v})) \cap V_{\text{unused}}^{(i)}, & \text{if } \hat{v} \in V_O \\ L^{(i-1)} \cap V_{\text{unused}}^{(i)}, & \text{otherwise,} \end{cases} \quad (16)$$

where  $i \in \{2, \dots, |V_O| + |V_M|\}$ ,  $L^{(1)} = \emptyset$ ,  $\hat{v}$  is the selected node in the  $(i - 1)$ -th step, and  $\mathcal{N}(\hat{v})$  is the set of (direct) neighbors of  $\hat{v}$ . Then, the likelihood  $p(\mathbf{O}_i^\pi | \tilde{\mathbf{S}}_{<i}^\pi, \boldsymbol{\theta}_i)$  in (15) is the same for all  $u \notin L^{(i)}$ , where  $u \in V_O$  and  $\pi(u) = i$ .

*Proof.* For the observable node  $u$  that does not belong to the

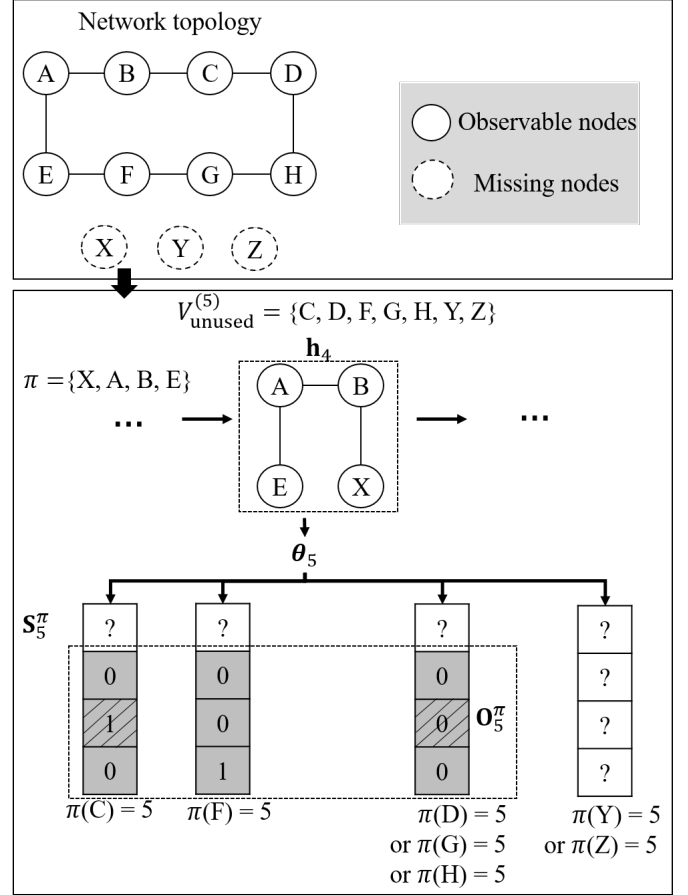


Fig. 5: An example illustrating the fifth inference step of DeepNC-LC, where nodes X, A, B, and E have been generated sequentially.

set  $L^{(i)}$  and is not generated for  $i - 1$  inference steps, all the observable entries in  $\mathbf{S}_i^\pi$  (i.e., entries in  $\mathbf{O}_i^\pi$ ) take the value of zeros since there is no associated edge. Thus, it follows that  $p(\mathbf{O}_i^\pi | \tilde{\mathbf{S}}_{<i}^\pi, \boldsymbol{\theta}_i) = \prod_{s_{i,j}^\pi=0} (1 - \boldsymbol{\theta}_i[j])$ , which is identical for all  $u \notin L^{(i)}$ , where  $u \in V_O$  and  $\pi(u) = i$ . This completes the proof of this lemma.  $\square$

Lemma 1 allows us to compute the likelihood  $p(\mathbf{O}_i^\pi | \tilde{\mathbf{S}}_{<i}^\pi, \boldsymbol{\theta}_i)$  only once for all nonselected observable nodes  $u \notin L^{(i)}$  when solving (15), which corresponds to the case where node D, G, or H is selected in the fifth step while  $L^{(5)} = \{C, F\}$ , indicating the set of nonselected neighbors of nodes A, B, and E (refer to Fig. 5).

Next, let us explain how to efficiently solve the problem in (15) without computing likelihoods  $p(\mathbf{O}_i^\pi | \tilde{\mathbf{S}}_{<i}^\pi, \boldsymbol{\theta}_i)$  for observable nodes. From Fig. 5, one can see that  $s_{5,3}^\pi$  (corresponding to entries with diagonal lines in  $\mathbf{O}_5^\pi$ ) is the only term that makes the difference between two sets  $\mathbf{O}_5^\pi$  for the cases when node C is selected and when either node D, G, or H is selected, which implies that it may not be necessary to compute the likelihoods of  $s_{5,2}^\pi$  and  $s_{5,4}^\pi$  for node selection.

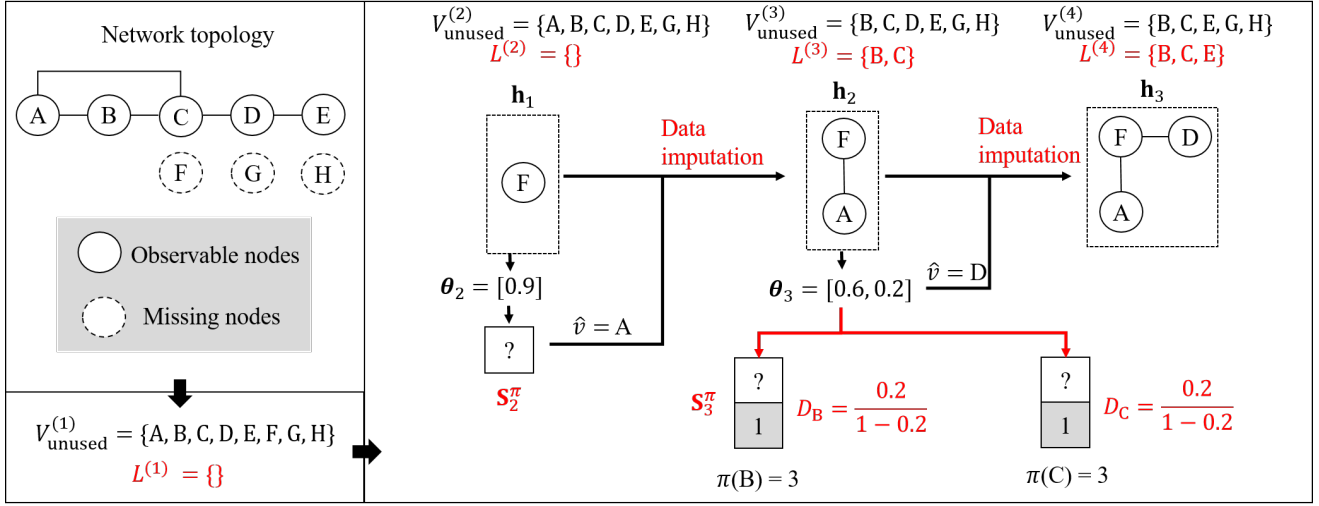


Fig. 6: An example illustrating the complexity reduction technique of DeepNC-LC, where the first three steps in Example 1 are revisited.

Thus, from the fact that most of the entries in  $\mathbf{O}_i^\pi$  tend to be *zeros* in many real-world networks that usually have a sparse structure, the computational complexity can be greatly reduced if we make comparison of likelihoods in (15) based only on the entries in  $\mathbf{O}_i^\pi$  that are *ones*. To this end, we eliminate all the terms  $(1 - \theta_i[j])$  corresponding to  $s_{i,j}^\pi = 0$  from  $p(\mathbf{O}_i^\pi | \tilde{\mathbf{S}}_{<i}^\pi, \theta_i)$  when a node  $v \in V_O \cap V_{\text{unused}}^{(i)}$  is selected. For computational convenience, we define

$$D_v = \frac{\prod_{s_{i,j}^\pi=1} \theta_i[j] \prod_{s_{i,j}^\pi=0} (1 - \theta_i[j])}{\prod_{s_{i,j}^\pi \in \mathbf{O}_i^\pi} (1 - \theta_i[j])} \quad (17)$$

$$= \prod_{s_{i,j}^\pi=1} \frac{\theta_i[j]}{(1 - \theta_i[j])}$$

for  $v \in V_O \cap V_{\text{unused}}^{(i)}$ . Since the denominator in (17) is the same for all  $v \in V_O \cap V_{\text{unused}}^{(i)}$ , it is obvious that  $\hat{v} = \arg \max_v D_v$  is the solution to (15). We note that computing  $D_v$  is less computationally expensive than computing  $p(\mathbf{O}_i^\pi | \tilde{\mathbf{S}}_{<i}^\pi, \theta_i)$  when the number of ones in  $\mathbf{O}_i^\pi$  is low. As a special case where all observable entries in  $\mathbf{S}_i^\pi$  take the value of zeros, the denominator in (17) is equivalent to  $p(\mathbf{O}_i^\pi | \tilde{\mathbf{S}}_{<i}^\pi, \theta_i)$ , which follows that  $D_u = 1$  due to the fact that a node  $u \notin L^{(i)}$  is selected. Thus, if  $D_v < 1$  for all  $v \in L^{(i)}$ , then the likelihood in (15) for selecting a node  $u \notin L^{(i)}$  is higher than that for selecting a node  $v \in L^{(i)}$ . In this case, we randomly choose a node  $\hat{v} \notin L^{(i)}$  without further computation from Lemma 1. In consequence, we compute  $D_v$  only for nodes in the set  $L^{(i)}$ , rather than computing  $D_v$  for all nodes in  $V_O \cap V_{\text{unused}}^{(i)}$ . The following example describes how the computational complexity can be reduced according to the aforementioned technique.

**Example 2:** Fig. 6 illustrates our complexity reduction technique for the first three steps in Example 1, where

changes are highlighted with red color. Assuming that node F is selected as the first node, we do not include any new nodes into  $L^{(2)}$  since F is a missing node. In the next step, when the node type is assumed to be observable, we randomly choose node A without computing the likelihood  $p(\mathbf{O}_2^\pi | \tilde{\mathbf{S}}_{<2}^\pi, \theta_2)$  due to the fact that  $L^{(2)} = \emptyset$ . Then, data imputation yields  $\tilde{\mathbf{S}}_2^\pi = [1]$ , which connects node A to node F. We create the set  $L^{(3)} = \{B, C\}$  by including neighbors of node A. Next, suppose that the node type is again observable. Then, instead of computing the term  $p(\tilde{\mathbf{S}}_3^\pi | \tilde{\mathbf{S}}_{<3}^\pi, \theta_3)$  in (14) six times as shown in Example 1, we only compute two terms  $D_B$  and  $D_C$ . Since  $D_B = D_C = \frac{\theta_3[2]}{(1 - \theta_3[2])} = \frac{0.2}{1 - 0.2} = 0.25$  from (17) and is lower than 1, we randomly choose one out of two observable nodes D and E that are not in the set  $L^{(3)}$  as the solution to (15) when  $i = 3$ .

#### 4.1.3 Stepwise Summary of DeepNC-LC

Now, we are ready to show the overall procedure of our proposed DeepNC-LC algorithm, which is summarized in Algorithm 1. We initially select the first node at random, and then start the inference process by identifying connections for the next node according to the following four stages:

1. Using two functions  $f_{\text{trans}}$  and  $f_{\text{out}}$  in (7) and (8), respectively, we obtain  $\theta_i$  (refer to lines 4–5).

2. Let  $m$  denote the cardinality of the set of unobservable nodes that can be potentially generated in the  $i$ -th step. We then randomly select the node type so that the selected node is unobservable with probability of  $m / (|V_O| + |V_M| - i + 1)$ . (refer to line 6).

3-1. If the type of observable nodes is selected, then we compute  $D_v$ , which is a function of  $\theta_i$ , according to (17) for all  $v \in L^{(i)}$ . When  $D_v < 1$  for all  $v \in L^{(i)}$  or  $L^{(i)} = \emptyset$ , we

**Algorithm 1: DeepNC-LC**


---

**Input:**  $G, M, f_{\text{out}}, f_{\text{trans}}$   
**Output:**  $\hat{\pi}$

- 1 **Initialization:**  $i \leftarrow 2; \mathbf{h}_0 \leftarrow$  random initialization;  
 $\tilde{\mathbf{S}}_1^\pi \leftarrow \emptyset; \hat{v} \leftarrow v \in V_O \cup V_M; \pi(\hat{v}) \leftarrow 1; L^{(1)} \leftarrow \emptyset;$   
Update  $L^{(i)}$  according to (16);
- 2 **function** DeepNC
- 3   **while**  $i \geq |V_O| + |V_M|$  **do**
- 4      $\mathbf{h}_{i-1} \leftarrow f_{\text{trans}}(\mathbf{h}_{i-2}, \tilde{\mathbf{S}}_{i-1}^\pi)$
- 5      $\boldsymbol{\theta}_i \leftarrow f_{\text{out}}(\mathbf{h}_{i-1})$
- 6     Select the node type
- 7     **if** a selected node is observable **then**
- 8       **for**  $v \in L^{(i)}$  **do**
- 9         Compute  $D_v$  according to (17)
- 10       **if** ( $D_v < 1$  for  $\forall v$  or  $L^{(i)} = \emptyset$ ) and  
 $L^{(i)} \neq V_O \cap V_{\text{unused}}^{(i)}$  **then**
- 11         Randomly select an observable node  
 $\hat{v} \notin L^{(i)}$
- 12       **else**
- 13          $\hat{v} \leftarrow \arg \max_v D_v$
- 14         Update  $L^{(i)}$  according to (16)
- 15       **else**
- 16         Randomly select an unobservable node  $\hat{v}$
- 17          $\tilde{\mathbf{S}}_i^\pi \leftarrow$  Impute  $\mathbf{S}_i^\pi$  according to (12)
- 18          $\pi(\hat{v}) \leftarrow i + 1$
- 19          $i \leftarrow i + 1$
- 20   **return**  $\hat{\pi}$

---

randomly select an observable node  $\hat{v} \notin L^{(i)}$  provided that  $L^{(i)} \neq V_O \cap V_{\text{unused}}^{(i)}$ . Otherwise, we select the node  $\hat{v}$  that maximizes  $D_v$ . Afterwards, we update  $L^{(i)}$  by including neighbors of the selected node  $\hat{v}$  (refer to lines 7–14).

3-2. If the type of missing nodes is selected, then we select one node  $\hat{v}$  randomly among all missing nodes that have not been generated until the  $i$ -th step. (refer to lines 15–16).

4. The data imputation process takes place before the next iteration of node generation. Finally, we update the node order  $\pi$  by including the selected node  $\hat{v}$  for the  $i$ -th step. The algorithm continues by repeating stages 1–4 and is terminated when a fully inferred sequence  $\mathbf{S}^\pi$  is generated (refer to lines 17–20).

## 4.2 Complexity Analysis

In this subsection, we analyze the computational complexity of the DeepNC-LC algorithm. We start by examining the complexity of each inference step  $i \in \{2, \dots, |V_O| + |V_M|\}$ . It is not difficult to show that the case where a node selected in the inference process is an observable one dominates the complexity. Note that it is possible to compute  $D_v$  in constant time as the average degree over a network is typically regarded as a constant [29]. Thus, the complexity

of this step is bounded by  $\mathcal{O}(|L^{(i)}|)$  since we exhaustively compute  $D_v$  over the nodes  $v \in L^{(i)}$ . The data imputation process is computable in constant time when parallelization can be applied since the Bernoulli trials are totally independent of each other. As our algorithm is composed of  $|V_O| + |V_M| - 1$  inference steps, the total complexity is finally given by  $\mathcal{O}((|V_O| + |V_M|)|L^{(i)}|)$ , which is rewritten as  $\mathcal{O}(|V_O| \cdot |L^{(i)}|)$  from the fact that  $|V_M| \ll |V_O|$ . The following theorem states a comprehensive analysis of the computational complexity.

**Theorem 1.** *Lower and upper bounds on the computational complexity of the proposed DeepNC-LC algorithm are given by  $\Omega(|V_O|)$  and  $\mathcal{O}(|V_O|^2)$ , respectively.*

*Proof.* The parameter  $L^{(i)}$  is the set of neighboring nodes to the observable nodes that have already been generated in the  $i$ -th step, while its cardinality depends on the network topology. For the best case where all nodes are isolated with no neighbors, we always have  $|L^{(i)}| = 0$  for each generation step; thus, each step is computable in constant time, yielding the total complexity of  $\Omega(|V_O|)$ . For the worst case, corresponding to a fully-connected graph, it follows that  $|L^{(i)}| = |V_O| + |V_M| - i$  for each generation step, thus yielding the total complexity of  $\mathcal{O}(|V_O|^2)$ . This completes the proof of this theorem.  $\square$

**Remark 1.** *Now, let us discuss how to examine a tighter bound on the computational complexity. Theorem 1 reveals that the computational complexity of the DeepNC-LC algorithm scales as  $\Theta(|V_O|^{1+\epsilon})$ , where  $0 \leq \epsilon \leq 1$  depends on a given network topology such as sparsity of networks. We shall validate this assertion via empirical evaluation for various datasets in the next section by identifying that  $\epsilon$  is indeed small, which implies that the complexity of DeepNC-LC is almost linear in  $|V_O|$ .*

## 5 EXPERIMENTAL EVALUATION

In this section, we first describe both synthetic and real-world datasets. We also present two state-of-the-art methods for network completion as a comparison. After presenting two performance metrics and our experimental settings, we intensively evaluate the performance of our DeepNC.

### 5.1 Datasets

Two synthetic and three real-world datasets across various domains (e.g., social, citations, and biological networks) are adopted as a series of homogeneous networks (graphs), denoted by  $G_I$ , and described in sequence. For all experiments, we treat graphs as undirected and only consider the largest connected component without any isolated nodes. The statistics of each dataset, including the number of similar graphs and the range of the number of nodes,

TABLE 2: Statistics of 5 datasets, where NG and NN denote the number of similar graphs and the range of the number of nodes in each dataset, respectively

| Name         | NG  | NN       |
|--------------|-----|----------|
| LFR          | 50  | 100-200  |
| B-A          | 50  | 100-200  |
| Protein      | 918 | 100-500  |
| Ego-CiteSeer | 737 | 50-399   |
| Ego-Facebook | 10  | 52-1,034 |

is described in Table 2. In the following, we summarize important characteristics of the datasets.

**Lancichinetti-Fortunato-Radicchi (LFR)** [30]. We construct a synthetic graph generated using the LFR model in which the degree exponent of a power-law distribution is set to 3. Other LFR parameters regarding community settings can be arbitrary since they do not affect our evaluation.

**Barabasi-Albert (B-A)** [15]. We construct another synthetic graph generated using the B-A model in which each node is connected to 4 existing nodes.

**Protein** [8]. The Protein structure is a biological network. Each protein is represented by a graph, where nodes are amino acids. Two nodes are connected if they are less than 6 Angstroms apart.

**Ego-CiteSeer** [7]. This CiteSeer dataset is a online citation network that is freely available. Nodes and edges represent publications and citations, respectively.

**Ego-Facebook** [9]. This Facebook dataset is a social friendship network extracted from Facebook. Nodes and edges represent people and friendship ties, respectively.

## 5.2 State-of-the-art Approaches

In this subsection, we present two state-of-the-art network completion approaches for comparison.

**KronEM** [5]. This approach aims to infer the missing part of a true network based solely on the connectivity patterns in the observed part via a generative graph model based on Kronecker graphs, where the parameters are estimated via an EM algorithm.

**EvoGraph** [31]. This study presents a graph upscaling method, called EvoGraph, that can upscale an original graph by attaching new nodes and edges to the observable network using an efficient preferential attachment mechanism. EvoGraph does not directly tackle the network completion problem, but can infer the missing nodes and edges while preserving network properties.

## 5.3 Performance Metrics

To assess the performance of our proposed method and other competing approaches, we need to quantify the degree of agreement between the recovered graph and the original

one. To this end, we adopt the following two performance metrics.

**Definition 2. Mean absolute error (MAE).** Let  $\hat{\mathbf{A}}^\pi$  and  $\mathbf{A}_T^\pi$  denote as the adjacency matrix of a recovered graph and the true graph, respectively, under a given node order  $\pi$ . Then, the MAE between two adjacency matrices is given by

$$\text{MAE}(\hat{\mathbf{A}}^\pi, \mathbf{A}_T^\pi) = \frac{\min_{\mathbf{P}} \|\hat{\mathbf{A}}^\pi - \mathbf{P}\mathbf{A}_T^\pi\mathbf{P}^\top\|_u}{(|V_O| + |V_M|)^2}, \quad (18)$$

where the permutation matrix  $\mathbf{P}$  is an  $(|V_O| + |V_M|) \times (|V_O| + |V_M|)$  matrix composed of 0's and 1's, with exactly one entry of 1 in each row and each column and 0's elsewhere, and  $\|\cdot\|_u$  can be any arbitrary matrix norm  $u$ .

Note that the term  $(|V_O| + |V_M|)^2$  in the denominator of (18) comes from the number of elements in the target matrix. In general, computing the MAE is equivalent to finding the solution to an inexact graph matching problem [12], which is proven to be NP-complete [32]. Exact graph matching algorithms have an exponential time complexity for the worst case. Hence, we adopt a fast graph matching method in [33] to measure the optimal correspondences between the two graphs, where the Frobenius norm is adopted.

**Definition 3. Graph edit distance (GED)** [13]. Given a set of graph edit operations, the GED between a recovered graph  $\hat{G}$  and the true graph  $G$  is defined as

$$\text{GED}(\hat{G}, G) = \min_{(e_1, \dots, e_k) \in \mathcal{P}(\hat{G}, G)} \sum_{i=1}^k c(e_i), \quad (19)$$

where  $\mathcal{P}(\hat{G}, G)$  denotes the set of edit paths transforming  $\hat{G}$  into a graph isomorphic to  $G$  and  $c(e) \geq 0$  is the cost of each graph edit operation  $e$ .

Note that only four operations are allowed in our setup, including vertex substitution, edge insertion, edge deletion, and edge substitution, and  $c(e)$  is identically set to one for all operations. Since the problem of computing the GED is NP-complete [34], we adopt an efficient approximation algorithm proposed in [35]. In our experiments, GED is normalized to be in the range  $[0, 2]$ .

## 5.4 Experimental Setup

Let us first describe the settings of neural networks. In our experiments, the function  $f_{\text{trans}}$  is implemented by using 4 layers of GRU cells with 128 dimensional hidden state; and the function  $f_{\text{out}}$  is implemented by using a two-layer multilayer perceptron with 64 dimensional hidden state and a sigmoid activation function. The Adam optimizer is used for minibatch training with a learning rate of 0.001, where each minibatch contains 32 graph sequences. We train the model for 32,000 batches in all experiments.

To test the performance of our method, we randomly select one graph from each dataset to act as the underlying true network  $G_T$ . From each dataset, we select all remaining similar graphs as training data  $G_I$  unless otherwise stated.

To create a partially observable network  $G$  from the true network, we adopt the following two graph sampling strategies in [36]. The first strategy, called *random node* (RN) sampling, selects nodes uniformly at random to create a sample graph. The second one, *forest fire* (FF) sampling, starts by picking a seed node uniformly at random and adding it to a sample graph (referred to as burning). Then, FF sampling burns a fraction of the outgoing links with nodes attached to them. This process is repeated recursively for each neighbor that is burned until no new node is selected to be burned. In our experiments, the partially observable network  $G_O$  consists of 70% of nodes via sampling unless otherwise specified.

## 5.5 Experimental Results

In this subsection, our empirical study is basically designed to answer the following four key research questions.

- Q1. How close is the performance of our DeepNC-LC method to that of DeepNC via exhaustive search (DeepNC-E)?
- Q2. How much does our DeepNC method improve the accuracy of network completion over the state-of-the-art approaches?
- Q3. How much is our DeepNC method beneficial to more difficult situations where either a large number of nodes and edges are missing or the training data are also incomplete?
- Q4. How much is DeepNC-LC scalable with the graph size?

To answer these questions, we carry out comprehensive experiments in terms of MAE and GED along with their standard deviations across five experiments using proper parameter settings.

### 5.5.1 Comparative Study Between DeepNC-E and DeepNC-LC (Q1)

In Fig. 7, we compare the MAE performance of DeepNC-E in Section 3.3 and DeepNC-LC in Section 4.1.3 according to the number of node permutations using two synthetic datasets, i.e., the LFR and B-A models, where two underlying true graphs  $G_T$  consisting of 100 and 200 nodes are selected from each of the two datasets. In these experiments, we only use the RN sampling strategy since the results from FF sampling follow similar trends. From the figure, we discuss our valuable findings as follows:

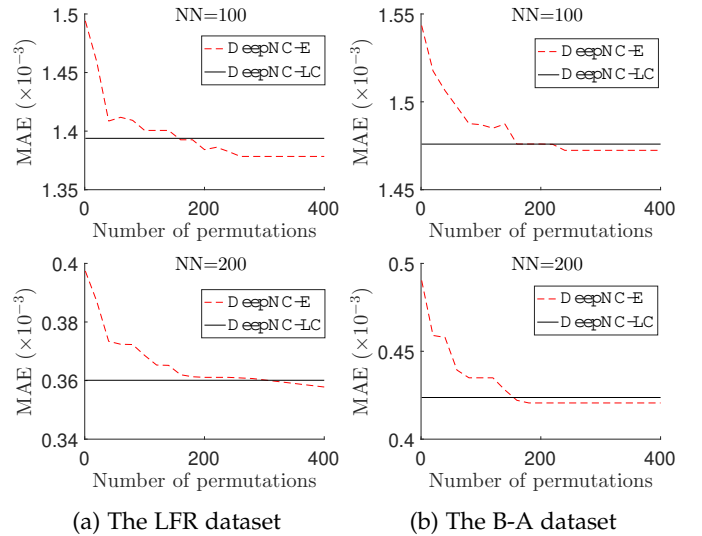


Fig. 7: MAE of DeepNC over the number of node permutations, where  $NN \in \{100, 200\}$ .

- The MAE of DeepNC-E is monotonically decreasing as the number of permutations increases, which demonstrates the convergence of DeepNC-E.
- For the LFR dataset, as depicted in Fig. 7a, the crossover points at which two curves for DeepNC-E and DeepNC-LC meet are found after 160 and 300 permutations when the true graph  $G_T$  is composed of 100 and 200 nodes, respectively. This implies that as the graph size increases, DeepNC-E necessitates more node permutations to guarantee the same performance as that of DeepNC-LC. In other words, DeepNC-E outperforms DeepNC-LC only when the number of permutations is sufficiently high. Similar trends are also found in Fig. 7b for the B-A dataset.
- From Section 3.3, it follows that the computational complexity of DeepNC-E via  $n$  node permutations is  $\mathcal{O}(n(|V_O| + |V_M|)^2)$ , where  $n$  should scale with  $|V_O|$  to assure satisfactory performance. This leads to the conclusion that as addressed in Remark 1, DeepNC-LC having an almost linear complexity in  $|V_O|$  is much more cost-effective than DeepNC-E under the same performance on the MAE.

### 5.5.2 Comparison With State-of-the-Art Approaches (Q2)

The performance comparison between DeepNC-LC and two state-of-the-art network completion methods, including KronEM [5] and EvoGraph [31], with respect to MAE and GED is presented in Tables 3 and 4, respectively, for all five datasets. In these experiments, to see the effect of the number training graphs on the performance of DeepNC-LC, we consider two cases such that training data  $G_I$  in each dataset correspond to 1) all remaining graphs except

TABLE 3: Performance comparison in terms of MAE ( $\times 10^{-3}$ , average  $\pm$  standard deviation)

| Dataset \ Method  | DeepNC-LC                  |                     | KronEM<br>( $Y$ )   | EvoGraph<br>( $Z$ ) | Gain (%)                     |                              |
|-------------------|----------------------------|---------------------|---------------------|---------------------|------------------------------|------------------------------|
|                   | all ( $X_1$ )              | single ( $X_2$ )    |                     |                     | $\frac{Y-X_1}{Y} \times 100$ | $\frac{Z-X_1}{Z} \times 100$ |
| LFR (RN)          | <b>0.3601</b> $\pm$ 0.0003 | 0.3847 $\pm$ 0.0651 | 0.3858 $\pm$ 0.0058 | 0.3881 $\pm$ 0.0042 | 6.65                         | 7.22                         |
| LFR (FF)          | <b>0.3599</b> $\pm$ 0.0001 | 0.3798 $\pm$ 0.0679 | 0.3847 $\pm$ 0.0074 | 0.3862 $\pm$ 0.0039 | 6.44                         | 6.81                         |
| B-A (RN)          | <b>0.4237</b> $\pm$ 0.0024 | 0.4994 $\pm$ 0.0553 | 0.5081 $\pm$ 0.0056 | 0.5163 $\pm$ 0.0016 | 16.62                        | 17.95                        |
| B-A (FF)          | <b>0.4173</b> $\pm$ 0.0085 | 0.4306 $\pm$ 0.0539 | 0.4979 $\pm$ 0.0022 | 0.5156 $\pm$ 0.0023 | 16.19                        | 19.06                        |
| Protein (RN)      | <b>1.1906</b> $\pm$ 0.0018 | 1.5286 $\pm$ 0.1107 | 1.7067 $\pm$ 0.0015 | 1.5502 $\pm$ 0.0009 | 30.24                        | 23.20                        |
| Protein (FF)      | <b>1.1918</b> $\pm$ 0.0010 | 1.4701 $\pm$ 0.1094 | 1.7160 $\pm$ 0.0022 | 1.5549 $\pm$ 0.0016 | <b>30.55</b>                 | <b>23.35</b>                 |
| Ego-CiteSeer (RN) | <b>0.2208</b> $\pm$ 0.0050 | 0.2233 $\pm$ 0.0190 | 0.2221 $\pm$ 0.0051 | 0.2247 $\pm$ 0.0008 | 0.60                         | 1.76                         |
| Ego-CiteSeer (FF) | <b>0.2208</b> $\pm$ 0.0050 | 0.2257 $\pm$ 0.0183 | 0.2343 $\pm$ 0.0051 | 0.2414 $\pm$ 0.0009 | 5.74                         | 8.51                         |
| Ego-Facebook (RN) | <b>0.7575</b> $\pm$ 0.0001 | 0.7655 $\pm$ 0.0333 | 0.7906 $\pm$ 0.0001 | 0.8114 $\pm$ 0.0002 | 4.19                         | 6.64                         |
| Ego-Facebook (FF) | <b>0.7574</b> $\pm$ 0.0001 | 0.7694 $\pm$ 0.1334 | 0.8045 $\pm$ 0.0001 | 0.7896 $\pm$ 0.0001 | 5.81                         | 4.09                         |

TABLE 4: Performance comparison in terms of GED (average  $\pm$  standard deviation)

| Dataset \ Method  | DeepNC-LC                  |                     | KronEM<br>( $Y$ )   | EvoGraph<br>( $Z$ ) | Gain (%)                     |                              |
|-------------------|----------------------------|---------------------|---------------------|---------------------|------------------------------|------------------------------|
|                   | all ( $X_1$ )              | single ( $X_2$ )    |                     |                     | $\frac{Y-X_1}{Y} \times 100$ | $\frac{Z-X_1}{Z} \times 100$ |
| LFR (RN)          | <b>0.3008</b> $\pm$ 0.0634 | 0.3120 $\pm$ 0.0638 | 0.3637 $\pm$ 0.0188 | 0.5855 $\pm$ 0.0080 | 17.29                        | 48.63                        |
| LFR (FF)          | <b>0.2915</b> $\pm$ 0.0182 | 0.3173 $\pm$ 0.0642 | 0.3508 $\pm$ 0.0295 | 0.6686 $\pm$ 0.0069 | 16.90                        | 56.40                        |
| B-A (RN)          | <b>0.1801</b> $\pm$ 0.0026 | 0.1901 $\pm$ 0.0304 | 0.1939 $\pm$ 0.0064 | 1.2135 $\pm$ 0.0017 | 7.08                         | <b>85.15</b>                 |
| B-A (FF)          | <b>0.1847</b> $\pm$ 0.0066 | 0.1900 $\pm$ 0.0188 | 0.1950 $\pm$ 0.0084 | 1.2002 $\pm$ 0.0079 | 5.27                         | 84.61                        |
| Protein (RN)      | <b>0.2664</b> $\pm$ 0.0064 | 0.3426 $\pm$ 0.0223 | 0.4107 $\pm$ 0.0106 | 0.3874 $\pm$ 0.0040 | <b>35.14</b>                 | 31.24                        |
| Protein (FF)      | <b>0.2683</b> $\pm$ 0.0065 | 0.2918 $\pm$ 0.0833 | 0.3940 $\pm$ 0.0047 | 0.2995 $\pm$ 0.0789 | 31.92                        | 10.43                        |
| Ego-CiteSeer (RN) | <b>0.3325</b> $\pm$ 0.0036 | 0.3378 $\pm$ 0.0058 | 0.3398 $\pm$ 0.0064 | 0.4517 $\pm$ 0.0090 | 2.15                         | 26.39                        |
| Ego-CiteSeer (FF) | <b>0.3284</b> $\pm$ 0.0036 | 0.3315 $\pm$ 0.0150 | 0.3304 $\pm$ 0.0183 | 0.3734 $\pm$ 0.0093 | 0.63                         | 12.06                        |
| Ego-Facebook (RN) | <b>0.5929</b> $\pm$ 0.0554 | 0.6198 $\pm$ 0.0798 | 0.7106 $\pm$ 0.0107 | 0.7699 $\pm$ 0.0059 | 16.55                        | 22.98                        |
| Ego-Facebook (FF) | <b>0.5816</b> $\pm$ 0.1534 | 0.6241 $\pm$ 0.1684 | 0.8025 $\pm$ 0.0126 | 0.6751 $\pm$ 0.0041 | 27.53                        | 13.85                        |

for the true graph  $G_T$  and 2) a randomly selected single graph, namely DeepNC-LC (all) and DeepNC-LC (single), respectively. Meanwhile, both KronEM and EvoGraph operate based on the partially observable graph  $G_O$  without any training phase. We would like to provide interesting observations in the following:

- For most cases, the performance of KronEM is better than that of Evograph. However, KronEM is inferior to EvoGraph in the case where the degree distribution of a network does not strictly follow the pure power-law degree distribution. For example, EvoGraph consistently outperforms KronEM in terms of both MAE and GED in the Protein dataset.
- The improvement rates of DeepNC-LC (all) over KronEM are up to 30.55% and 35.14% in terms of MAE and GED, respectively. These maximum gains are achievable when the Protein dataset is used. Since DeepNC-LC (all) outperforms all state-of-the-art methods for all types of synthetic and real-world datasets, this observation reveals the robustness of our method toward various network topologies.
- Both DeepNC-LC (all) and DeepNC-LC (single) are

not sensitive to sampling strategies for creating a partially observable network, whereas the performance of EvoGraph depends on which sampling strategy is adopted. Specifically, the case via FF sampling mostly exhibits better performance than that via RN sampling when EvoGraph is used due to the fact that FF sampling strategy tends to preserve the network properties such as the degree distribution [36], which is essential in upscaling the underlying graph. This result displays the robustness of our DeepNC-LC method to graph samplings.

- DeepNC-LC (single) typically shows a marginal degradation on the MAE and GED compared to DeepNC-LC (all); thus, our approach requiring additional training phase does not contain any technical limitations in this context. It is worthwhile to highlight that DeepNC-LC (single) still outperforms the state-of-the-art methods for all the datasets except for Ego-CiteSeer.

### 5.5.3 Applicability to More Difficult Situations (Q3)

In Section 5.5.3, our DeepNC-LC algorithm is compared to the two state-of-the-art network completion methods in

TABLE 5: Performance comparison in terms of MAE when 70% of nodes is missing ( $\times 10^{-3}$ , average  $\pm$  standard deviation)

| Method \ Dataset | DeepNC-LC (X)              | KronEM (Y)          | EvoGraph (Z)        | Gain (%)                   |                            |
|------------------|----------------------------|---------------------|---------------------|----------------------------|----------------------------|
|                  |                            |                     |                     | $\frac{Y-X}{Y} \times 100$ | $\frac{Z-X}{Z} \times 100$ |
| LFR              | <b>0.3781</b> $\pm$ 0.0003 | 0.6091 $\pm$ 0.0008 | 0.6159 $\pm$ 0.0041 | <b>37.92</b>               | <b>38.61</b>               |
| B-A              | <b>0.4286</b> $\pm$ 0.0061 | 0.6336 $\pm$ 0.0136 | 0.6330 $\pm$ 0.0119 | 32.34                      | 32.28                      |
| Protein          | <b>1.2372</b> $\pm$ 0.0409 | 1.9402 $\pm$ 0.0710 | 1.6027 $\pm$ 0.0259 | 36.23                      | 22.81                      |
| Ego-CiteSeer     | <b>0.3805</b> $\pm$ 0.0141 | 0.5032 $\pm$ 0.0098 | 0.5600 $\pm$ 0.0041 | 24.38                      | 32.05                      |
| Ego-Facebook     | <b>0.7840</b> $\pm$ 0.0189 | 0.9392 $\pm$ 0.0078 | 0.9483 $\pm$ 0.0070 | 16.53                      | 17.32                      |

TABLE 6: Performance comparison in terms of GED when 70% of nodes is missing (average  $\pm$  standard deviation)

| Method \ Dataset | DeepNC-LC (X)              | KronEM (Y)          | EvoGraph (Z)        | Gain (%)                   |                            |
|------------------|----------------------------|---------------------|---------------------|----------------------------|----------------------------|
|                  |                            |                     |                     | $\frac{Y-X}{Y} \times 100$ | $\frac{Z-X}{Z} \times 100$ |
| LFR              | <b>0.3117</b> $\pm$ 0.0660 | 0.6096 $\pm$ 0.0047 | 0.6324 $\pm$ 0.0134 | 48.87                      | 50.72                      |
| B-A              | <b>0.1874</b> $\pm$ 0.0042 | 0.6805 $\pm$ 0.1258 | 0.4741 $\pm$ 0.1133 | <b>72.46</b>               | <b>60.47</b>               |
| Protein          | <b>0.2802</b> $\pm$ 0.0085 | 0.5029 $\pm$ 0.0803 | 0.4180 $\pm$ 0.0760 | 44.28                      | 32.97                      |
| Ego-CiteSeer     | <b>0.3479</b> $\pm$ 0.0094 | 0.6211 $\pm$ 0.0624 | 0.7670 $\pm$ 0.0752 | 43.99                      | 54.64                      |
| Ego-Facebook     | <b>0.6284</b> $\pm$ 0.0597 | 0.8840 $\pm$ 0.1087 | 1.2505 $\pm$ 0.0781 | 28.91                      | 49.75                      |

more difficult settings that often occur in real environments: 1) the case where a large portion of nodes is missing and 2) the case where training graphs are also partially observed. In these experiments, we only apply the RN sampling strategy since the results from FF sampling follow similar trends.

First, we create a partially observable network  $G_O$  consisting of only 30% of nodes from the underlying true graph  $G_T$  via sampling. The performance comparison between DeepNC-LC and two state-of-the-art methods with respect to MAE and GED is presented in Tables 5 and 6, respectively, for all five datasets. From Tables 3–6, it is observed that such a high missingness of nodes and associated edges results in significant performance degradation for KronEM and EvoGraph, while DeepNC-LC is robust to the degree of observability in networks.

Next, we perform RN sampling so that only a part of nodes in training graphs can be observable. In Fig. 8, we compare the GED of DeepNC-LC and two state-of-the-art methods, where the degree of observability in training graphs is given by  $\{90, 95, 100\}\%$  in our method. The results exhibit that DeepNC-LC still outperforms the state-of-the-art methods, only excluding the B-A and Ego-CiteSeer datasets showing a slight inferiority to KronEM when 90% of nodes in training graphs is observable.

#### 5.5.4 Scalability (Q4)

We empirically show the average runtime complexity via experiments using the three sets of B-A synthetic graphs, where the number of connections from each new node to existing nodes, denoted by  $c$ , is set to 2, 4, and 8. In each graph set, the number of nodes,  $|V_O| + |V_M|$ , varies from 20

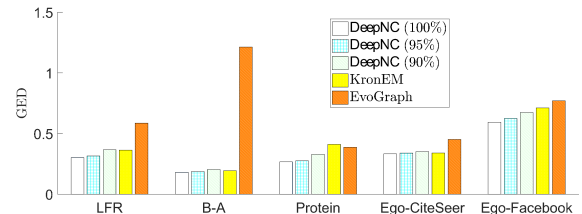


Fig. 8: Performance comparison in terms of GED, where the degree of observability in training graphs is given by  $\{90, 95, 100\}\%$ .

to 200 in an increment of 20; and 30% of nodes and their associated edges are deleted by RN sampling to create partially observable networks. Other parameter settings follow those in Section 5.4. In Fig. 9, we illustrate the log-log plot of the execution time in seconds versus  $|V_O|$ , where each point represents the average complexity over 10 executions of DeepNC-LC. In the figure, dotted lines are also shown from the analytical result with a proper bias, showing a tendency that slopes of the lines for  $c \in \{2, 4, 8\}$  are approximately given by 1.19, 1.32, and 1.46, respectively. This indicates that the computational complexity of DeepNC-LC is dependent on the average degree in a given graph. Moreover, it is asserted that an almost linear complexity in  $|V_O|$ , i.e.,  $\Theta(|V_O|^{1+\epsilon})$  for a small  $\epsilon > 0$ , is attainable since the slopes are at most 1.46 even for the ultra-dense graph case corresponding to  $c = 8$ .

## 6 CONCLUDING REMARKS

In this paper, we introduced a novel method, termed DeepNC, that infers both missing nodes and edges of the underlying network via deep learning. Specifically, we

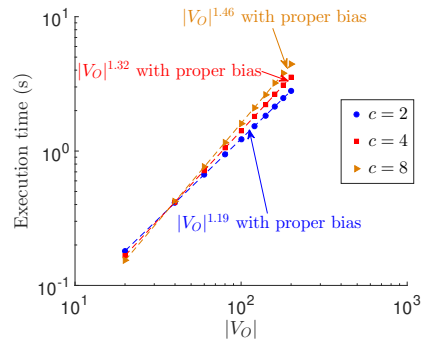


Fig. 9: The computational complexity of DeepNC-LC, where the log-log plot of the execution time versus  $|V_O|$  is shown.

presented an approach to first learning a likelihood over edges via an RNN-based generative graph model by using structurally similar graphs as training data and then inferring the missing parts of the network by applying an imputation strategy of the missing data. Furthermore, we proposed DeepNC-LC, a DeepNC algorithm whose runtime complexity is almost linear in  $|V_O|$ . Using various synthetic and real-world datasets, we demonstrated that our DeepNC approach not only remarkably outperforms KronEM and EvoGraph methods but also is robust to many difficult situations that often occur in real environments such as the cases where either a large portion of nodes is missing or training graphs are partially observed. Additionally, we analytically and empirically showed the scalability of our DeepNC-LC algorithm.

Potential avenues of future research include the design of a unified framework for improving the performance of various downstream mining and learning tasks such as multi-label node classification, community detection, and influence maximization when DeepNC is adopted in partially observable networks. This would not be straightforward since task-specific preprocessing should be accompanied with network completion to guarantee satisfactory performance of each task.

## ACKNOWLEDGMENTS

This work was supported by the Basic Science Research Program through the National Research Foundation of Korea (NRF) funded by the Ministry of Education (2017R1D1A1A09000835). Won-Yong Shin is the corresponding author.

## REFERENCES

- [1] G. Kossinets, "Effects of missing data in social networks," *Soc. Netw.*, vol. 28, no. 3, pp. 247–268, Jul. 2006.
- [2] A. Acquisti, L. Brandimarte, and G. Loewenstein, "Privacy and human behavior in the age of information," *Science*, vol. 347, no. 6221, pp. 509–514, Jan. 2015.
- [3] R. Dey, Z. Jelveh, and K. Ross, "Facebook users have become more private: A large-scale study," in *Proc. IEEE Int. Conf. Pervasive Comput. Commun. Worksh.*, Lugano, Switzerland, Mar. 2012, pp. 346–352.
- [4] J. H. Koskinen, G. L. Robins, P. Wang, and P. E. Pattison, "Bayesian analysis for partially observed network data, missing ties, attributes and actors," *Soc. Netw.*, vol. 35, no. 4, pp. 514–527, Oct. 2013.
- [5] M. Kim and J. Leskovec, "The network completion problem: Inferring missing nodes and edges in networks," in *Proc. 2011 SIAM Int. Conf. Data Mining (SDM '11)*, Mesa, AZ, USA, Apr. 2011, pp. 47–58.
- [6] C. Tran, W.-Y. Shin, and A. Spitz, "Community detection in partially observable social networks," *arXiv preprint arXiv:1801.00132*, 2017.
- [7] P. Sen, G. Namata, M. Bilgic, L. Getoor, B. Galligher, and T. Eliassi-Rad, "Collective classification in network data," *AI Magazine*, vol. 29, no. 3, pp. 93–106, 2008.
- [8] P. D. Dobson and A. J. Doig, "Distinguishing enzyme structures from non-enzymes without alignments," *J. Molecular Bio.*, vol. 330, no. 4, pp. 771–783, Jul. 2003.
- [9] A. L. Traud, E. D. Kelsic, P. J. Mucha, and M. A. Porter, "Comparing community structure to characteristics in online collegiate social networks," *SIAM Rev.*, vol. 53, no. 3, pp. 526–543, Aug. 2011.
- [10] J. You, R. Ying, X. Ren, W. Hamilton, and J. Leskovec, "GraphRNN: Generating realistic graphs with deep auto-regressive models," in *Proc. Int. Conf. Machine Learning (ICML '18)*, Stockholm, Sweden, Jul. 2018, pp. 5694–5703.
- [11] A. Bojchevski, O. Shchur, D. Zügner, and S. Günnemann, "NetGAN: Generating graphs via random walks," in *Proc. Int. Conf. Machine Learning (ICML '18)*, Stockholm, Sweden, Jul. 2018, pp. 609–618.
- [12] L. A. Zager and G. C. Verghese, "Graph similarity scoring and matching," *Appl. Math. Lett.*, vol. 21, no. 1, pp. 86–94, Jan. 2008.
- [13] A. Sanfeliu and K.-S. Fu, "A distance measure between attributed relational graphs for pattern recognition," *IEEE Trans. Syst. Man Cybernetics*, vol. SMC-13, no. 3, pp. 353–362, Jun. 1983.
- [14] P. Erdos and A. Rényi, "On random graphs I," *Publ. Math. Debrecen*, vol. 6, pp. 290–297, 1959.
- [15] A.-L. Barabási and R. Albert, "Emergence of scaling in random networks," *Science*, vol. 286, no. 5439, pp. 509–512, Oct. 1999.
- [16] J. Leskovec, D. Chakrabarti, J. Kleinberg, C. Faloutsos, and Z. Ghahramani, "Kronecker graphs: An approach to modeling networks," *J. Mach. Learning Res.*, vol. 11, pp. 985–1042, Feb. 2010.
- [17] M. Simonovsky and N. Komodakis, "GraphVAE: Towards generation of small graphs using variational autoencoders," in *Proc. Int. Conf. Artificial Neural Netw. Machine Learning (ICANN '18)*, Rhodes, Greece, Oct. 2018, pp. 412–422.
- [18] J. You, B. Liu, Z. Ying, V. Pande, and J. Leskovec, "Graph convolutional policy network for goal-directed molecular graph generation," in *Proc. Advances Neural Inf. Processing Syst. (NIPS '18)*, Montreal, Canada, Dec. 2018, pp. 6410–6421.
- [19] D. Zhou, L. Zheng, J. Xu, and J. He, "Misc-GAN: A multi-scale generative model for graphs," *Fronti. Big Data*, vol. 2, pp. 3:1–3:10, Apr. 2019.
- [20] Y. Li, O. Vinyals, C. Dyer, R. Pascanu, and P. Battaglia, "Learning deep generative models of graphs," *arXiv preprint arXiv:1803.03324*, 2018.
- [21] H.-H. Chen, L. Gou, X. Zhang, and C. L. Giles, "Capturing missing edges in social networks using vertex similarity," in *Proc. 6th Int. Conf. Knowl. Capture (K-CAP '11)*, Alberta, Canada, Jun. 2011, pp. 195–196.
- [22] F. Buccafurri, G. Lax, A. Nocera, and D. Ursino, "Discovering missing me edges across social networks," *Inf. Sci.*, vol. 319, pp. 18–37, Oct. 2015.

- [23] R. Eyal, A. Rosenfeld, S. Sina, and S. Kraus, "Predicting and identifying missing node information in social networks," *ACM Trans. Knowl. Disc. Data*, vol. 8, no. 3, pp. 14:1–14:35, Jun. 2014.
- [24] S. Sina, A. Rosenfeld, and S. Kraus, "Solving the missing node problem using structure and attribute information," in *Proc. 2013 IEEE/ACM Int. Conf. Advances Social Netw. Analysis Mining (ASONAM '13)*, Niagara Falls, Canada, Aug. 2013, pp. 744–751.
- [25] H. A. Almohamad and S. O. Duffuaa, "A linear programming approach for the weighted graph matching problem," *IEEE Trans. Pattern Analysis Machine Intel.*, vol. 15, no. 5, pp. 522–525, May 1993.
- [26] T. H. McCormick, M. J. Salganik, and T. Zheng, "How many people you know?: Efficiently estimating personal network size," *J. Am. Stat. Assoc.*, vol. 105, no. 489, pp. 59–70, Sep. 2010.
- [27] J. Chung, C. Gulcehre, K. Cho, and Y. Bengio, "Empirical evaluation of gated recurrent neural networks on sequence modeling," in *Proc. Deep Learning and Representation Learning Worksh.*, Montreal, Canada, Dec. 2014.
- [28] S. Hochreiter and J. Schmidhuber, "Long short-term memory," *Neural Comput.*, vol. 9, no. 8, pp. 1735–1780, Nov. 1997.
- [29] M. E. Newman, "Random graphs as models of networks," *Proc. National Acad. Sci.*, vol. 99, no. 1, pp. 2566–2572, 2002.
- [30] A. Lancichinetti and S. Fortunato, "Benchmarks for testing community detection algorithms on directed and weighted graphs with overlapping communities," *Phys. Rev. E*, vol. 80, no. 1, pp. 016118:1–016118:8, Apr. 2009.
- [31] H. Park and M.-S. Kim, "EvoGraph: An effective and efficient graph upscaling method for preserving graph properties," in *Proc. 24th ACM SIGKDD Int. Conf. Knowl. Disc. Data Mining (KDD '18)*, London, United Kingdom, Aug. 2018, pp. 2051–2059.
- [32] A. M. Abdulkader, "Parallel algorithms for labelled graph matching," *Colorado School of Mines*, 1998.
- [33] Y. Lu, K. Huang, and C.-L. Liu, "A fast projected fixed-point algorithm for large graph matching," *Pattern Recognition*, vol. 60, pp. 971–982, Dec. 2016.
- [34] Z. Zeng, A. K. H. Tung, J. Wang, J. Feng, and L. Zhou, "Comparing stars: On approximating graph edit distance," *Proc. VLDB Endow.*, vol. 2, no. 1, pp. 25–36, Aug. 2009.
- [35] K. Riesen and H. Bunke, "Approximate graph edit distance computation by means of bipartite graph matching," *Image Vision Comput.*, vol. 27, no. 7, pp. 950–959, Jun. 2009.
- [36] J. Leskovec and C. Faloutsos, "Sampling from large graphs," in *Proc. 12th ACM SIGKDD Int. Conf. Knowl. Disc. Data Mining (KDD '06)*, Philadelphia, PA, USA, Aug. 2006, pp. 631–636.